An Investigation of Thin-Film Ni−Fe Oxide Catalysts for the Electrochemical Evolution of Oxygen

Mary W. Louie and Alexis T. Bell*

Joint Center for Artificial Photosynthesis, Materials Science Division, Lawrence Berkeley National Laboratory, California 94720, United States

Department of Chemical and Biomolecular Engineering, University of California , Berkeley, Berkeley, California 94720, United States

ⓢ *Supporting Information*

ABSTRACT: A detailed investigation has been carried out of the structure and electrochemical activity of electrodeposited Ni−Fe films for the oxygen evolution reaction (OER) in alkaline electrolytes. Ni−Fe films with a bulk and surface composition of 40% Fe exhibit OER activities that are roughly 2 orders of magnitude higher than that of a freshly deposited Ni film and about 3 orders of magnitude higher than that of an Fe film. The freshly deposited Ni film increases in activity by as much as 20-fold during exposure to the electrolyte (KOH); however, all films containing Fe are stable as deposited. The oxidation of $Ni(OH)_2$ to NiOOH in Ni films occurs at potentials below the onset of the OER. Incorporation of Fe into the film increases the potential at which $Ni(OH)_2$/NiOOH redox occurs and decreases the average oxidation state of Ni in NiOOH. The Tafel slope (40 mV dec^{-1}) and reaction order in OH$^-$ (1) for the mixed Ni−Fe films (containing up to 95% Fe) are the same as those for aged Ni films. In situ Raman spectra acquired in 0.1 M KOH at OER potentials show two bands characteristic of NiOOH. The relative intensities of these bands vary with Fe content, indicating a change in the local environment of Ni−O. Similar changes in the relative intensities of the bands and an increase in OER activity are observed when pure Ni films are aged. These observations suggest that the OER is catalyzed by Ni in Ni−Fe films and that the presence of Fe alters the redox properties of Ni, causing a positive shift in the potential at which $Ni(OH)_2$/NiOOH redox occurs, a decrease in the average oxidation state of the Ni sites, and a concurrent increase in the activity of Ni cations for the OER.
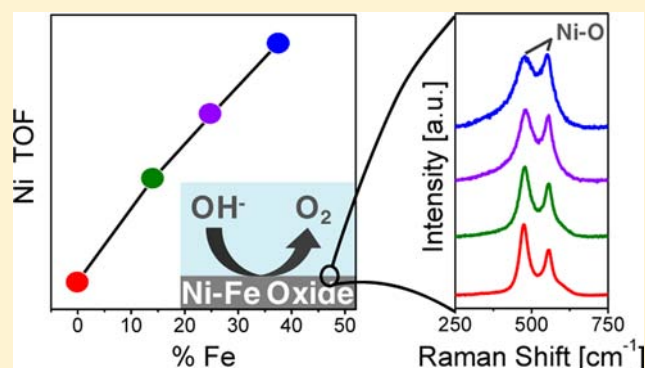
1. INTRODUCTION

The electrolysis of water to form hydrogen and oxygen offers a possible means for storing energy obtained from intermittent sources such as the sun.[1,2] However, the electrolysis of water requires voltages in substantial excess of the thermodynamic potential for water-splitting ($H_2O \rightarrow H_2 + 1/2O_2$), 1.23 V, due primarily to the slow kinetics of the oxygen evolution reaction (OER).[1] At present, the most active catalysts for the OER are RuO_2 and IrO_2, but even these operate with overpotentials in excess of 200 mV (at a current density of 10 mA cm^{-2}).[1−3] Moreover, the scarcity of Ru and Ir makes it impractical to use the metals on a large scale. For these reasons, there has been considerable interest in the discovery and development of OER catalysts based on earth-abundant metals.

A review of the literature suggests that Ni−Fe catalysts offer a promising alternative to catalysts based on precious metals.[4−12] The lowest overpotential reported, ~230 mV at 10 mA cm^{-2} for electrodeposited Ni−Fe films,[4] is comparable to overpotentials of 280 and 220 mV for chemically synthesized IrO_2 and RuO_2 films.[3] It is also notable that Ni−Fe catalysts are significantly more active for oxygen evolution than either Ni or Fe alone, which exhibit overpotentials of 350−450 and ~500

mV, respectively, at 10 mA cm^{-2}.[13,14] While the beneficial effects of Fe on the OER activity of Ni have been reported in a number of studies,[7,10−15] little is known about the structural or chemical characteristics of Ni−Fe catalysts, particularly under conditions where the OER occurs. A small number of in situ spectroscopic studies have been carried out but yield contradictory results. Ni−Fe catalysts (9−20 at % Fe) characterized by either in situ X-ray absorption or Mossbauer spectroscopy, at potentials relevant for oxygen evolution, have been found to contain Ni(III), but the oxidation state of Fe is not clearly defined; some authors conclude that it is Fe(III)[6,15] and others, that it is Fe(IV).[16−18]

We report here a structural and electrochemical investigation of Ni−Fe catalysts used for the OER in alkaline electrolyte. The structure of the electrodeposited Ni−Fe film was characterized in situ by Raman spectroscopy as a function of the applied potential, and the surface compositions were determined by ex situ X-ray photoelectron spectroscopy (XPS). The observed Raman characteristics of the Ni−Fe series combined with the

Ni redox behavior and the kinetic parameters for the OER are used to correlate structural characteristics of the catalyst under reaction conditions with the catalyst composition and the catalytic activity.

2. EXPERIMENTAL SECTION

2.1. Electrocatalyst Preparation. Electrocatalyst films containing Ni and/or Fe were prepared by electrodeposition onto gold electrodes. These gold substrates (99.95%, DOE Business Center for Precious Metals Sales and Recovery (BCPMSR)) were sheathed in Teflon, leaving exposed surfaces which were either 4 or 5 mm in diameter. Prior to electrodeposition, the gold substrates were polished with alumina slurries, from 5 μm down to 50 nm in particle size, with 15 min of sonication in water after each polish. Electrodes which were used for Raman measurements were additionally roughened, in KCl (Sigma-Aldrich, P3911), using a previously reported electrochemical cycling procedure in order to produce substrates that are ideal for surface-enhanced Raman measurements.[19] (For details see section S1.1, Supporting Information [SI].) Both smooth and roughened gold substrates were used for electrochemical measurements; the OER activity of these substrates was verified to be negligible compared to that of the films measured in this work (Figure S5, SI).

Electrolyte solutions for electrodeposition were obtained by dissolving nickel sulfate hexahydrate (≥99.99% trace metals basis, Sigma-Aldrich 467901) and/or iron sulfate heptahydrate (ACS Reagent ≥99.0%, Sigma-Aldrich 215422) in ultrapure water (18.2 MΩ, EMD Millipore). The metal concentrations were varied between 0 and 0.01 M such that deposition baths with less than 50% Fe contained 0.01 M Ni and a varying Fe concentration, and baths with greater than 50% Fe contained 0.01 M Fe and a varying Ni concentration. Prior to dissolution of the appropriate quantities of sulfate salts, the water was sparged with nitrogen gas for 1 h to prevent oxidation of Fe(II) to Fe(III) and enable well-controlled depositions. Films were electrodeposited galvanostatically with a cathodic current density of 50 μA cm^{-2} applied for 1125 s and with nitrogen gas flowing in the headspace. The potential of the working electrode was monitored using a Ag/AgCl reference electrode with 4 M KCl filling solution (Pine RREF0021) or a leakless Ag/AgCl electrode with 3.4 M KCl filling solution (eDaq ET072). The counterelectrode was a coiled Pt wire (99.95%, DOE BCPMSR) which was routinely soaked in 5 M nitric acid to remove any deposited Ni or Fe.

Aged Ni films were prepared by immersion of as-deposited Ni films, without potential cycling, in 10 M KOH solutions for over 24 h. Immersion of the films was carried out in Teflon or polypropylene cells/containers so as to minimize contaminants from glassware. Electrochemical and in situ Raman characterization of these films was carried out after the Ni redox peaks and OER currents observed in the cyclic voltammograms were stable, typically 5−10 cycles.

2.2. Physical Characterization. The compositions and quantities of the electrodeposited materials were determined by elemental analysis. Electrodeposited films were dissolved by sonication in high-purity 5 M HNO$_3$ (Sigma-Aldrich 84385 or EMD Millipore NX0407). These solutions were diluted and adjusted such that the final solutions contained 5% w/w HNO$_3$ and 1000 ppb of yttrium internal standard (Sigma Aldrich 01357). Samples were characterized by inductively coupled plasma optical emission spectroscopy (ICP Optima 7000 DV, Perkin-Elmer). Calibration solutions contained 5% w/w HNO$_3$, 1000 ppb Y, and both Ni and Fe, each with concentrations between 0 and 2000 ppb (Sigma-Aldrich 28944 and 43149 for Ni and Fe sources, respectively). On the basis of these measurements, we estimate the thicknesses of Ni−Fe films to be ~25 and ~70 nm when deposited on roughened and polished gold substrates, respectively. (For details see section S2.2, SI.)

The surface compositions of the electrodeposited Ni−Fe films were determined by X-ray photoelectron spectroscopy (XPS). Both as-deposited Ni−Fe films and films which were polarized under OER conditions (335 mV overpotential in 0.1 M KOH) for 1−2 h were examined. The XPS measurements were carried out with a Kratos Axis Ultra spectrometer using a monochromatic Al Kα source (15 mA,

15 kV). The instrument base pressure was 10^{-9} Torr, and the charge neutralizer system was used for all measurements. High-resolution spectra for Ni 2p, Fe 2p, O 1s, and C 1s were collected using a pass energy of 20 eV, a step energy of 50 meV, and dwell times of 200−400 ms. Angle-resolved XPS measurements were carried out by varying the electron takeoff angle between 0° and 75° with respect to the sample normal. The resulting spectra were analyzed using CasaXPS (Casa Software, Ltd.). A standard Shirley baseline with no offset was used for background correction. In the case of Fe 2p spectra, an additional correction was necessary due to the presence of a Ni LMM Auger peak. (For details see sections S4.2−S4.3, SI.) The C 1s spectrum for adventitious carbon (284.8 eV) was used for charge correction.

2.3. Electrochemical Characterization. Electrochemical characterization of the Ni−Fe catalysts was carried out in KOH electrolytes (ACS reagent ≥85%, Sigma-Aldrich 221473) with concentrations of 0.1−4.6 M in ultrapure water. (This KOH source is specified by the supplier to have ≤0.001% Fe and ≤0.001% Ni.) A Hg/HgO reference electrode (CH Instruments, ET072) with 1 M KOH filling solution was used throughout the experiments; the filling solution was exchanged before each experiment and measured against a second, unused Hg/HgO reference electrode stored in 1 M KOH. The counter electrode was a coiled Pt wire, cleaned routinely by nitric acid to remove any accumulated Ni or Fe deposits. All potentials reported in this work, unless otherwise noted, are measured against this Hg/HgO (1 M KOH) reference which has a potential of 0.098 V vs the normal hydrogen electrode (NHE). The equilibrium potential for oxygen evolution at any given pH is therefore $(1.23 - 0.098 - 0.059 \times pH)$ V.

Two electrochemical cells were used to measure the current−voltage characteristics of the Ni−Fe catalysts. One was a home-built Teflon cell[20] which was designed for efficient collection of Raman signals. The second was a rotating disk electrode (RDE) apparatus (Pine Instruments) employed for additional electrochemical characterization of Ni−Fe films, particularly for acquiring data for analysis of OER kinetics in the absence of mass transfer effects. Measurements were carried out using either a Gamry Reference 600 or a BioLogic VSP potentiostat. IR compensation was applied at 85−95% using the ohmic resistance determined by AC impedance methods. Specifically, impedance spectra were obtained at 0 ± 10 mV (vs Hg/HgO) between 1 MHz and 10 mHz, and the ohmic contribution was estimated from the Nyquist plots. For 1 and 0.1 M KOH electrolytes, the ohmic resistances were typically ~5 and ~40 Ω, respectively. When necessary, compensation of the remaining 5−15% of the ohmic resistance was applied manually to the current−potential data. This procedure, while having negligible impact on the shape of the redox features, was necessary for acquiring accurate OER currents and therefore Tafel slopes, particularly for measurements in electrolytes with lower KOH concentrations and/or for electrocatalysts with high OER activity. It should be noted that the compensated resistance is noticeably higher during Raman spectra acquisition in 0.1 M KOH (100−200 Ω), since immersion of the objective reduces the effective cross section for ionic conduction.

2.3.1. Surface Area. The surface areas of the films were estimated by measuring the electrochemical capacitance of the film−electrolyte interface in the double-layer regime of the voltammograms. Using 0.1 M KOH, the electrode was potentiostatically cycled, typically between and 0.1 and 0.16 V vs Hg/HgO (1 M KOH), at scan rates between 1 and 10 mV s^{-1} until the measured voltammograms had stabilized. The positive and negative capacitance currents at the center of the potential window were averaged and plotted against the scan rate to extract the measured capacitance. The surface areas reported were obtained by using a specific capacitance of 60 μF cm^{-2} for oxides.[21] (Representative plots are provided in section S2.3 of the SI.) The measured currents were normalized by this area to obtain the specific current density. The challenges associated with determining the surface area of catalysts have been reviewed by Trasatti and Petrii.[21] Extracted values of the specific current density, while reliable for comparing across the Ni−Fe system, should be used with care when comparing to other catalysts reported in the literature. Additional discussion is provided in the SI, section S2.3.
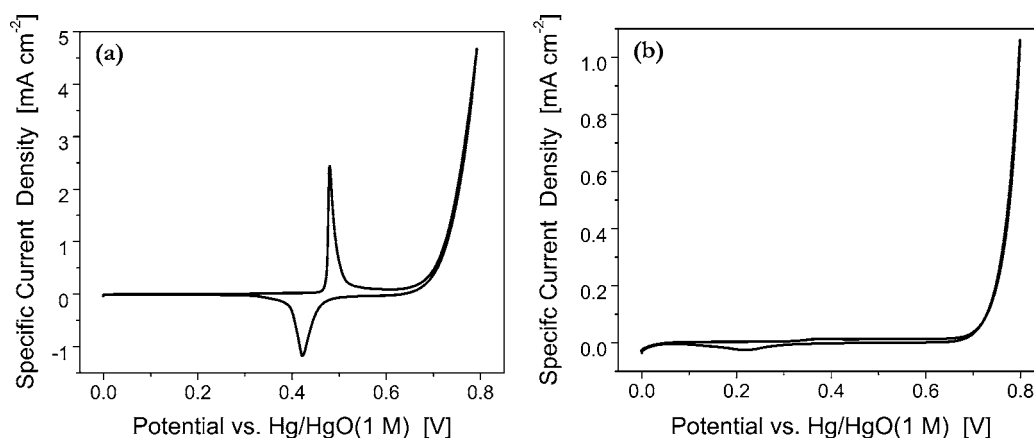
12330

dx.doi.org/10.1021/ja405351s | *J. Am. Chem. Soc.* 2013, 135, 12329−12337

Figure 1. Cyclic voltammograms for (a) Ni and (b) Fe films deposited on an Au substrate, measured in 0.1 M KOH at room temperature with 10 mV s^{-1} scan rate and 2400 rpm. The equilibrium potential for OER is 0.365 V vs Hg/HgO (1 M KOH).

2.3.2. Cyclic Voltammograms. Cyclic voltammograms were recorded between 0 and 0.7−0.8 V vs Hg/HgO in 0.1 M KOH, with the high-potential limit adjusted so as to minimize the amount of current driven through the high-activity catalysts. For the same reason, the potential window was adjusted by ~60 mV per unit pH, since higher OER currents were observed at higher KOH concentrations. Voltammograms were recorded until the redox peaks and the oxygen evolution currents show negligible change, typically 5−10 cycles, with the exception of as-deposited Ni films which slowly age/transform in alkaline electrolytes.[22] While low scan rates are desirable for obtaining current−voltage curves for kinetic analysis, we chose a scan rate of 10 mV s^{-1} to limit the overall time spent under oxygen evolution conditions. At slower scan rates, increasingly more bubbles formed under OER conditions and collected on or near the electrode surface. The accumulation of bubbles on the electrode surface caused a drop in the measured current due to coverage of the active sites and/or to the additional ohmic resistance not accounted for by the uncompensated resistance values measured under non-OER conditions. For experiments carried out in the RDE apparatus, the rotation rate was varied between 0 and 2400 rotations per minute (RPM).

The activity for the OER was determined from cyclic voltammograms by reading the specific current density at either a constant overpotential of 300 mV or the overpotential at a constant specific current density of 10 mA cm^{-2}. The Tafel slope was obtained from data collected by rotating the electrode at 2400 rpm to reduce mass transport effects and to increase the potential window for Tafel analysis. In selecting the region for the Tafel fit, we avoided high potentials at which oxygen bubble evolution causes mass transport limitations, and low potentials at which the redox transition for Ni(II)/Ni(III) occurs.

The dependence of the OER current density on the concentrations of OH$^-$ and O$_2$ was determined. KOH concentrations of 0.1, 0.22, 0.46, 1.0, 2.2, and 4.6 M were used; these correspond to pHs of 13, 13.3, 13.7, 14, 14.3 and 14.7, respectively. Cyclic voltammograms were collected for each electrolyte concentration; measurements were repeated for the high and low concentrations of 0.1 and 4.6 M (pH 13 and 14.7) at the end of the concentration series to verify stability of the catalyst films with changing KOH concentration. To examine effect of O$_2$ concentration, voltammograms were measured in 0.1 M KOH electrolyte sparged for one hour with either N$_2$ or O$_2$ prior to measurement. It should be noted that KOH concentrations below pH 12.5 resulted in gradual changes in the nickel redox features and OER current with time.

2.3.3. Calculation of the Turnover Frequency. The turnover frequency (TOF) based on Ni sites can be computed in two ways. Taking the Ni in the entirety of the film to be catalytically active, a lower limit, TOF$_{min}$, can be calculated using the number of Ni atoms determined by elemental analysis. On the other hand, the upper limit, TOF$_{max}$, can be estimated by taking the measured surface area of a film and computing the number of Ni atoms at the surface using a value of

6.4 × 10^{14} Ni atoms per cm^2 area[23] and the surface fraction of Ni as determined by XPS. Although TOF$_{min}$ and TOF$_{max}$ differ by 1−2 orders of magnitude, the dependence of TOF on composition is not affected. Here, we report TOF$_{min}$, but both TOF$_{min}$ and TOF$_{max}$ are presented in the SI section S7.

2.4. In Situ Raman Spectroscopy. Raman spectra were acquired under controlled electrochemical potentials using a homemade Teflon cell, which contained a working electrode (4 mm Au, Teflon-sheathed) oriented at the bottom of the cell.[20] We employed a water-immersion objective (70× mag., N. A. = 1.23, LOMO) which was protected from the corrosive KOH electrolytes by a 0.001-in. thick fluorinated ethylene propylene film (McMaster-Carr) or 0.0005-in. thick Teflon film (American Durafilm); a droplet of water was placed between the objective lens and the film to retain the high illumination/collection efficiencies. Additional details are provided in ref 20.

Raman spectra were collected using a confocal Raman microscope (LabRAM HR, Horiba Yvon Jobin) with a wavelength of 633 nm and a power of 1−3 mW at the objective. The spot size of the laser beam is estimated to be between 1 and 2 μm. Acquisition times for Ni−Fe films were typically 3 s for spectral range of 1100 cm^{-1} window. Using a 600 g/mm grating, the spectral resolution is ~1 cm^{-1}. Spectral shifts were calibrated routinely against the value of 520.7 cm^{-1} for a silicon wafer. Raman spectra were collected at selected potentials as the potential of working electrode was scanned at a rate of 1 mV s^{-1}. Raman spectra were not background-corrected due to the complexity of SERS backgrounds. When quantifying relative changes in the peak heights of Raman bands (carried out for cases when surface-enhancement contributions are minimized), a linear background correction was used. The sampling depth/volume of Ni−Fe films by surface-enhanced Raman spectroscopy is discussed in the SI, section S5.5.

3. RESULTS AND DISCUSSION

3.1. Electrochemical Characteristics of Ni−Fe Films. Representative cyclic voltammograms for Ni and Fe films, i.e., the end-members of the catalyst series, are shown Figure 1. The cyclic voltammogram for an as-deposited Ni film in 0.1 M KOH (Figure 1a) exhibits two primary characteristics, a redox couple at 0.47 V vs Hg/HgO (1 M KOH) and a positive (oxidation) current visible at overpotentials greater than 0.65 V. Both are well-known features for Ni electrodes in alkaline electrolytes. The redox peaks are attributed to the transformation between Ni(OH)$_2$ and NiOOH,[14,22] which proceeds as Ni(OH)$_2$ + OH$^-$ ↔ NiOOH + H$_2$O + e$^-$ in alkaline electrolytes. Oxidation currents at higher potentials are due to the evolution of oxygen, 4OH$^-$ → O$_2$ + 2H$_2$O + 4e$^-$.

The cyclic voltammogram for Fe in 0.1 M KOH (Figure 1b) shows an oxidation current attributed to the OER visible at

potentials positive of 0.7 V. No redox transitions for Fe are observed in this potential window, consistent with previous reports in literature, since the oxidation of metallic Fe to Fe(II)/Fe(III) oxides/hydroxides occur at potentials between −0.5 V and −1.2 V vs Hg/HgO (1 M).[13,24] The reduction peak observed at 0.22 V is that for the underlying gold substrate (Figure S1, SI); this feature is also present in the case of Ni films but not apparent in Figure 1a due to the significantly higher currents observed compared to that of Fe.

The cyclic voltammograms for mixed Ni−Fe films are characterized by two primary features: one for the $Ni(OH)_2$/NiOOH redox couple and the other for the OER. Two measures were defined for the OER activity, one being the specific current density at a constant overpotential of 300 mV and the other the overpotential at a specific current density of 10 mA cm^{-2}. A plot of these two parameters as a function of the surface composition of the Ni−Fe films, as determined by X-ray photoelectron spectroscopy (section S.4, SI), reveals that the OER current density varies across 3 orders of magnitude with composition (Figure 2). The maximum specific current
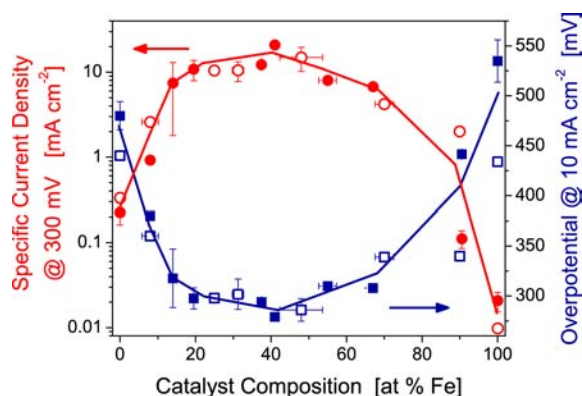

Figure 2. Oxygen evolution activity of electrodeposited Ni−Fe catalysts, taken at 300 mV overpotential and 10 mA cm^{-2} specific current density, as a function of composition in 0.1 M KOH. Filled and open markers correspond to measurements taken using rotating and stationary Au working electrode substrates for which electrodeposited films are ∼70 and ∼25 nm thick, respectively.

density of 20 mA cm^{-2} and the minimum overpotential of 280 mV were measured at a composition of 40% Fe. The

observation of this dramatic enhancement of the OER activity indicates that Ni−Fe catalysts do not behave as simple mixtures of the end-members and that interaction between Ni and Fe results in an improvement in the rate of oxygen evolution. It is notable that, across a composition range of 15−50% Fe, the specific current density only varies by 2-fold (between 10 and 20 mA cm^{-2}) and the overpotential by 20 mV. This behavior is consistent with the discrepancies found in literature[4−10] regarding the composition of highest OER activity for the Ni−Fe system; the optimum composition has been reported to be as low as 10% Fe[6,7] and as high as 50% Fe.[4]

The voltammograms for the Ni−Fe series differ noticeably in their $Ni(OH)_2$/NiOOH redox characteristics (Figure 3a). As more Fe is incorporated into the Ni−Fe film, the $Ni(OH)_2$/NiOOH redox couple shifts to higher potentials, consistent with previous reports,[4,5,7,10] and the peak area decreases (Figure 3a). At an Fe content of 41% or greater, the oxidation wave is no longer visible due to its coincidence with the rapid rise in the OER current, which increases initially with increasing Fe content (Figure 2). However, films for which both oxidation and reduction peaks are visible indicate that the two shift in tandem and have comparable integrated areas (Figure S4a, SI). Therefore, we used the reduction peak to quantify changes in the redox characteristics of Ni−Fe films as a function of composition. A strong linear correlation is observed between the reduction peak potential and the Fe content (Figure 3b); the reduction peak shifts to positive potentials by as much as 150 mV relative to that for pure Ni films when the film contains 70% Fe. This shift in the redox potential implies that the electrochemical oxidation of $Ni(OH)_2$ to NiOOH is suppressed by the presence of Fe. The reduction peaks were integrated in order to determine the extent of Ni reduction/oxidation in the Ni−Fe films. As shown in Figure 3c for pure Ni films deposited atop roughened Au substrates, the charge passed during redox is greater than can be accounted for by assuming a one-electron redox reaction; we find that 1.2 electrons are transferred per Ni atom in a redox cycle. (The number of Ni atoms deposited was measured by elemental analysis.) This result is consistent with reports that the Ni can exist as γ-NiOOH in which Ni has an average oxidation state as high as 3.7,[14,25−28] and therefore that the α-$Ni(OH)_2$/γ-NiOOH transformation can involve the transfer of up to 1.7 electrons per Ni atom. Figure 3c shows that the number of electrons transferred during $Ni(OH)_2$/NiOOH redox depends strongly on the Fe content, decreasing
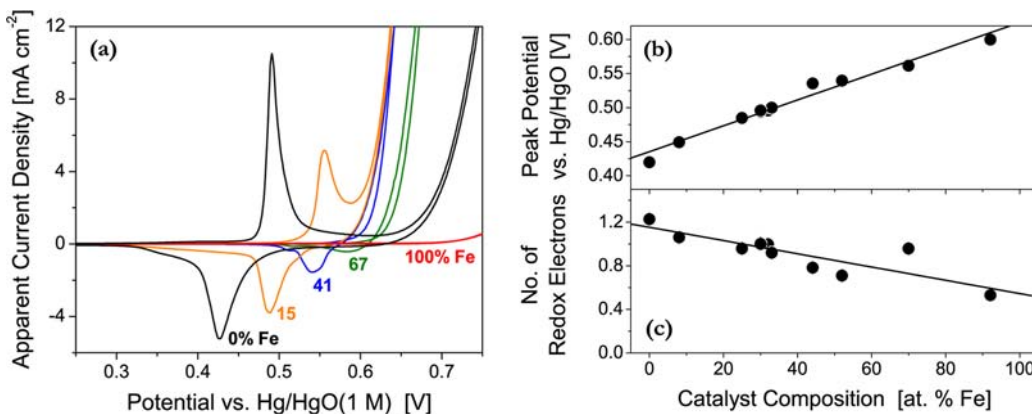

Figure 3. Effect of Fe on the $Ni(OH)_2$/NiOOH redox couple in 0.1 M KOH. (a) Selected cyclic voltammograms for Ni−Fe films on polished gold substrates collected at 10 mV s^{-1} and 2400 rpm, (b) reduction peak potential, and (c) the number of electrons transferred during redox as a function of Fe content, shown for films on roughened gold substrates. Lines in (b) and (c) indicate linear fits to the data.

from ~1.2 for pure Ni films to ~0.5 for films containing 90% Fe. Since all the Ni atoms in the films undergo redox, this implies that addition of 90% Fe causes the average oxidation state of Ni to decrease from ~3.2 to ~2.5. We note that for thicker films deposited onto polished substrates the number of electrons per Ni involved in redox decreased with Fe content; however, in this case not all of the Ni in the film underwent redox. (Additional discussion provided in section S2.4 of the SI.)

3.2. Electrochemical Characteristics of Aged Ni Films.

Ni electrodes are known to age in alkaline electrolytes.[23,25,29] Aging is attributed to the transformation of the α-Ni(OH)$_2$/ γ-NiOOH couple to the ordered and compact β-Ni(OH)$_2$/ β-NiOOH couple. Associated with this transformation is an anodic shift in the Ni(II)/Ni(III) redox potential, a decrease in the Ni oxidation state, and an increase in the OER activity.[14,22−25,29,30] This phenomenon was also observed in our Ni films. The cyclic voltammograms for as-deposited and aged Ni films are compared in Figure 4. Here, the redox peaks
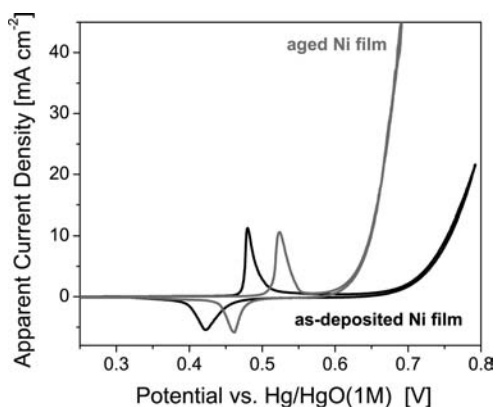
Figure 4. Cyclic voltammograms for as-deposited and aged Ni films in 0.1 M KOH. The aged Ni films exhibit a higher redox potential for the Ni(OH)$_2$/NiOOH transition and a higher activity for the OER. Voltammograms were collected at 10 mV s^{-1} and 2400 rpm.

for aged Ni films occur at potentials 40 mV higher than those for as-deposited Ni films, and the OER activity is ~4 mA cm^{-2} (at 300 mV overpotential), 20-fold higher than that for as-deposited films. As we will show later, we use the characteristics of both types of Ni films to elucidate the behavior of the Ni−Fe system.

It has been reported that potential cycling of nominally pure Ni films for extended periods of time can result in the incorporation of Fe present as impurities in the KOH electrolyte. In our measurements, the concentrations of Fe in freshly deposited and aged Ni films are comparable and close to the detection limit for elemental analysis. Therefore, although the possibility of Fe incorporation cannot be eliminated, the dramatic change in the current−voltage characteristics during aging is likely not due to a change in Fe content. We attribute the negligible change in the Fe content to the absence of an applied potential during the aging process.

3.3. In Situ Raman Spectroscopy of Ni−Fe Catalysts.

Figure 5 shows a series of Raman spectra for a Ni film deposited onto a Au substrate and immersed in 0.1 M KOH, acquired as a function of the applied potential (vs Hg/HgO) during an oxidation sweep. The spectral features and their changes with potential are consistent with the transformation of Ni(OH)$_2$ to NiOOH which starts at a potential of 0.47 V vs
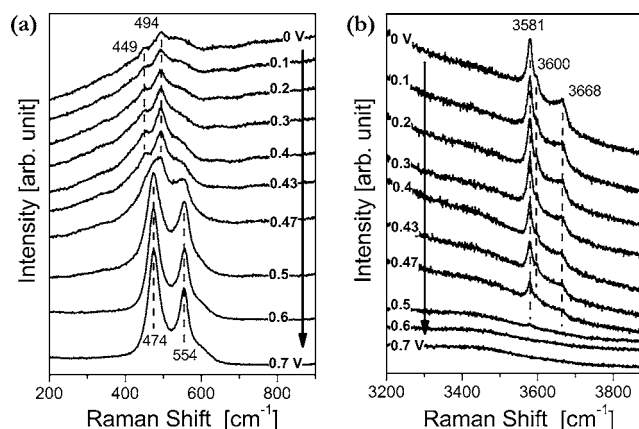
Figure 5. In situ Raman spectra collected at (a) low and (b) high wavenumbers for Ni films atop a roughened Au substrate as a function of potential vs Hg/HgO(1 M KOH) in 0.1 M KOH, for which the equilibrium potential for the OER is 0.365 V.

Hg/HgO (as shown in Figure 1a). The band at 449 cm^{-1} is attributable to α-Ni(OH)$_2$ and β-Ni(OH)$_2$, both of which exhibit Ni−O bands in the range 445−465 cm^{-1}.[22,26,31−33] The band at 494 cm^{-1} and the broad, underlying feature centered at ~530 cm^{-1} are best assigned to defective or disordered Ni(OH)$_2$.[22,26,32,34−37] Previous studies have reported that disordered or doped Ni(OH)$_2$ exhibits a Ni−O vibration that is shifted positively by as much as ~65 mV of the band at 445− 465 cm^{-1}. (Additional discussion of this feature is given in sections S5.3 and S5.4.1 of the SI.) The latter feature indicates that the Ni films produced in this study are not perfectly crystalline but, instead, are disordered or defective. At high wavenumbers (Figure 5b), the bands at 3581−3668 cm^{-1} can be attributed to O−H vibrations of Ni(OH)$_2$. β-Ni(OH)$_2$ exhibits a single O−H band at 3580 cm^{-1}, whereas α-Ni(OH)$_2$ displays broader bands at 3625−3670 cm^{-1}.[22,26,31,38] A band at 3580 cm^{-1} has also been reported for the so-called α-Ni(OH)$_2$ phases, a consequence of the variability in the structure of the more disordered α-Ni(OH)$_2$. The work of Bernard et al.[38] clearly shows that phases between completely disordered α-Ni(OH)$_2$ (with no O−H band at 3580 cm^{-1}) and perfectly crystalline β-Ni(OH)$_2$ (with a single O−H band at 3580 cm^{-1}) exist. Therefore, on the basis of the features observed in the O−H regime (Figure 5b), we conclude that our electro-deposited films are not composed of perfectly crystalline β-Ni(OH)$_2$. Rather α-Ni(OH)$_2$ or some form of disordered β-Ni(OH)$_2$ is present.

The pair of bands at 474 and 554 cm^{-1}, observed at 0.5− 0.7 V vs Hg/HgO (Figure 5a), are attributed to Ni−O vibrations in NiOOH. These two vibrations are known to have high Raman cross section due to resonance effects,[26] consistent with the higher signal-to-noise ratio for these bands compared to the bands for the Ni(OH)$_2$ phase. Both γ-NiOOH and β-NiOOH exhibit a pair of bands at these wavenumbers.[23,31,33] However, the relative intensities of the two bands have been found to differ; specifically, in β-NiOOH, the ratio of the intensity of the 474 cm^{-1} band to that of the 554 cm^{-1} band is lower than that for γ-NiOOH.[22,23,37] On the basis of the relative intensities of these two bands, the assignments for the Ni(OH)$_2$ phase, and the redox potential measured for these films (Figure 4), we attribute these bands primarily to γ-NiOOH. The presence of γ-NiOOH is consistent with the Ni oxidation state of 3.2 estimated for as-deposited Ni films

(Figure 3c). The absence of O—H vibrations for NiOOH (Figure 5b, 0.5—0.7 V) is consistent with previous reports. The broad bands present at 3100—3600 cm^{-1} are well-known characteristics of water.[22,39] (Figure S21, SI)

In the case of Fe, Figure 6, an intense band at 571 cm^{-1} is observed at 0 V. This band shows very little change with the
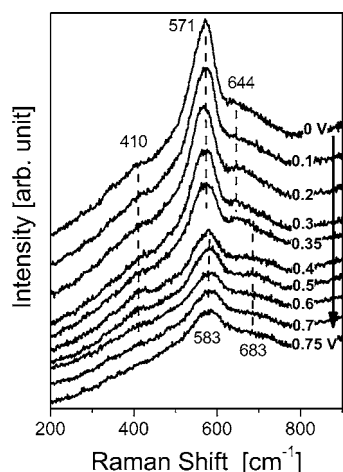

Figure 6. In situ Raman spectra collected for Fe films deposited on a roughened Au substrate, shown as a function of potential vs Hg/HgO (1 M KOH) in 0.1 M KOH. The equilibrium potential for the OER is 0.365 V.

applied potential, consistent with the electrochemical characteristics (Figure 1b). An apparent decrease in the intensity of these bands at potentials above 0.35 V is a consequence of the increased background due to the electrochemical oxidation of the underlying gold substrate. (Figure S17, SI) Additional bands are observed at 410 cm^{-1} and in the range of 650—720 cm^{-1}; these features change slightly in their relative intensities with potential but are too low in intensity for reliable analysis. Unlike the Raman spectra for Ni films, the Fe phase displays no structural O—H stretches. Identification of the bands observed for Fe films is rather difficult owing to the many possible iron oxide and oxyhydroxide phases, many of which are structurally similar.[40] The primary band at 571 cm^{-1} is closest in shift to those for α-FeOOH (560 cm^{-1}) and Fe$_3$O$_4$ (553 cm^{-1}), and the low-intensity band at 410 cm^{-1} matches that of α-Fe$_2$O$_3$ (409 cm^{-1}).[41] The bands at 650—720 cm^{-1} may originate from Fe$_3$O$_4$, γ-Fe$_2$O$_3$ and γ-FeOOH which exhibit bands at 670, 650—740, and 660 cm^{-1}, respectively.[41] (See additional discussion in section S5.2 of the SI.)

We captured the main features of the Ni—Fe system by plotting the Raman spectra of Ni—Fe films as functions of composition at two different potentials, 0.2 and 0.6 V vs Hg/HgO, the latter of which corresponds to an OER overpotential of 0.235 V (Figures 7 and 8, respectively). These two potentials are selected to show composition effects at potentials below and above the Ni(OH)$_2$/NiOOH redox potential for each catalyst.

At 0.2 V, the Raman features for mixed Ni—Fe films can be assigned to those of the end-members. The sharp bands of Ni(OH)$_2$ (450 and 494 cm^{-1}) are present for films with up to 32% Fe (Figure 7a) and disappear at higher Fe contents. On the other hand, the broad band of Ni(OH)$_2$ ($\sim$530 cm^{-1}) remains at these intermediate compositions but has shifted to higher wavenumbers ($\sim$560 cm^{-1}). Contributions from the Fe
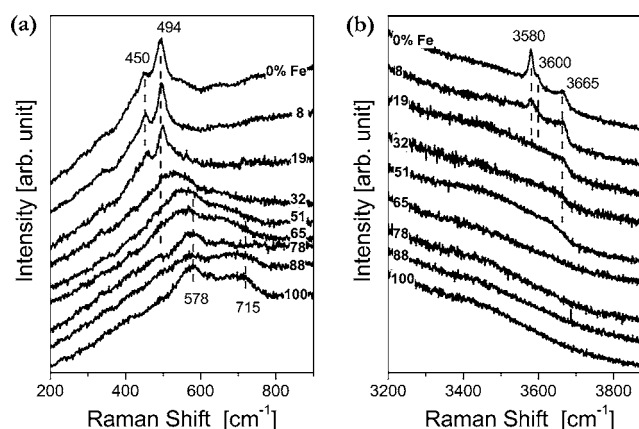

Figure 7. In situ Raman spectra collected for Ni—Fe catalysts, as a function of composition, in 0.1 M KOH at a potential of 0.2 V vs Hg/HgO (1 M KOH), shown for the (a) low and (b) high wavenumber regions.
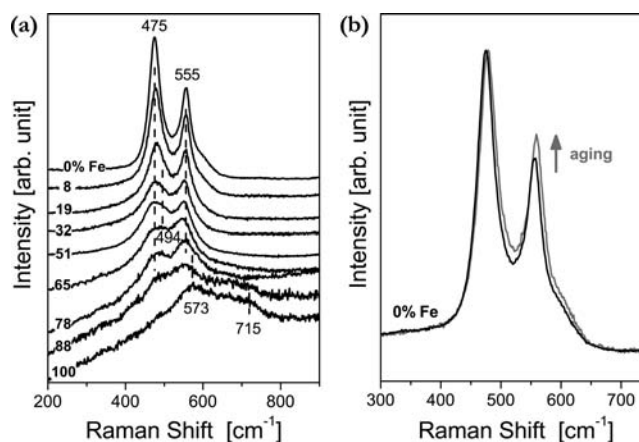

Figure 8. In situ Raman spectra collected in 0.1 M KOH at an OER overpotential of 0.235 V, or 0.6 V vs Hg/HgO (1 M KOH), for (a) Ni—Fe films as a function of composition and (b) an aged Ni film, shown in comparison to the as-deposited Ni film from (a).

phase are also visible at 578 and 650—720 cm^{-1}. The disappearance of the sharp Ni(OH)$_2$ bands and the persistence of the broad underlying band suggests that Ni—Fe is disordered. Spectra collected at higher wavenumbers (Figure 7b) support this conclusion, namely, that the sharp band at 3580 cm^{-1} corresponding to the ordered β-Ni(OH)$_2$ phase disappears with increasing Fe content, leaving only a broad feature at 3500—3660 cm^{-1} for films with 19—51% Fe.

Under an oxygen evolution potential of 0.6 V vs Hg/HgO (Figure 8a), the two characteristic bands for NiOOH (at 475 and 555 cm^{-1} for the Ni film) are visible for films with as much as 90% Fe, owing to the high Raman cross section of NiOOH.[26] These two bands appear to merge with increasing Fe content, and an additional band at 494 cm^{-1} is apparent, as a shoulder on the band at 475 cm^{-1}, for films containing 30—80% Fe. The most dramatic effect of composition is the change in relative intensities of the pair of NiOOH bands; the 555 cm^{-1} band increases in intensity with Fe incorporation. This change in the relative intensities is readily apparent for films with as little as 19% Fe and clearly visible for films with higher Fe contents despite the appearance of the 494 cm^{-1} band. At Fe contents of 90% or higher, features associated with Fe (and Au) phases, at 573 and 650—720 cm^{-1}, can be seen. It should be

noted that the high Raman cross section of the NiOOH vibrations limits the amount of information we can extract from the Fe phases in catalysts with low-to-intermediate Fe contents. However, we can reliably analyze the NiOOH bands even for Ni−Fe films with small quantities of Ni. We verified that the changes in NiOOH bands and the presence of the 494 cm^{-1} band are not artifacts of the Fe and/or Au phases at ∼573 cm^{-1} which overlap with the NiOOH band at 555 cm^{-1} (Figure S23, SI). We also show here the effect of aging on the two NiOOH bands (Figure 8b); as is the case with Fe incorporation, aging of a Ni film also results in an increase in the intensity of the 555 cm^{-1} band relative to the 475 cm^{-1} band.

With the exception of the feature at 494 cm^{-1}, no bands attributable to new phases of Ni and/or Fe were observed. In particular, NiFe$_2$O$_4$, which contains 67% Fe(III) and 33% Ni(II), exhibits high-intensity Raman bands at approximately 490 and 700 cm^{-1}.[42,43] This pair of bands was not observed at 0.2 V, at which Ni exists as Ni(II). At 0.6 V, this pair of bands, particularly the band at 700 cm^{-1}, was not observed even for high Fe content (for which contribution of the high-intensity NiOOH bands are minimal). The absence of these bands is particularly noteworthy because it has been suggested that NiFe$_2$O$_4$ is the cause of high OER activities in mixed Ni−Fe catalysts.[6] However, our in situ Raman observations do not show evidence for NiFe$_2$O$_4$ in highly active Ni−Fe catalysts.

3.4. Analysis of OER Kinetics.

The Tafel slope and the reaction order in OH$^-$ for the Ni−Fe catalyst series are shown in Figure 9. The Tafel slopes for aged Ni films and mixed
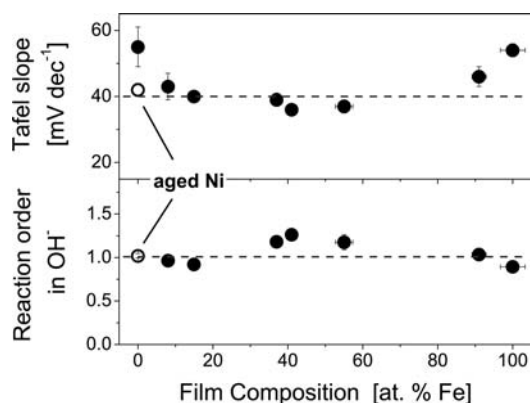

Figure 9. Extracted Tafel slopes and reaction orders in the concentration of OH$^-$ for the Ni−Fe films, taken from measurements in 0.1−4.6 M KOH. Dashed lines for a Tafel slope of 40 mV dec^{-1} and a reaction order of unity are shown for reference.

Ni−Fe films are close to 40 mV dec^{-1}, while those for as-deposited Ni films and pure Fe films are ∼55 mV dec^{-1}. The reaction order in OH$^-$ is unity for all films, with the exception of as-deposited Ni films for which the reaction order could not be determined due to the gradual aging of the films in alkaline electrolytes. The OER current was found to be independent of O$_2$ concentration in the electrolyte solution. (See additional discussion in section S3.2 of the SI.) The Tafel slope of 40 mV dec^{-1} and reaction order of 1 in OH$^-$ for aged Ni and mixed Ni−Fe has also been found by Lyons and Brandon for nickel electrodes;[14] these two kinetic parameters have been rationalized using a reaction pathway composed of an initial reversible discharge of an OH$^-$ ion followed by a rate-limiting electron transfer step which results in the formation of a physisorbed hydrogen peroxide intermediate. The observation

that the kinetic parameters for aged Ni and for mixed Ni−Fe films are the same implies a common rate-limiting step for these catalysts. That is, the enhancement in the OER activity due to Fe incorporation into the film results from an increase in the rate of the rate-limiting step rather than from a change in the reaction pathway. That the kinetic parameters for mixed Ni−Fe are the same as those for aged Ni but not as-deposited Ni implies that aged Ni films and mixed Ni−Fe films share a common reaction pathway.

3.5. Implications for OER Activity.

Raman spectroscopy indicates that, under OER potentials, Ni in Ni−Fe catalysts is present as NiOOH and that the structure of this phase is modified dramatically as a consequence of Fe incorporation. The increase in the intensity of the 560 cm^{-1} band relative to the 480 cm^{-1} band is clearly noticeable, even for Fe contents as low as 20%. This change in the intensity ratio is reminiscent of that observed during the transformation of γ-NiOOH to β-NiOOH, the latter of which has been widely agreed to be the preferred phase for catalyzing the OER,[14,23,44,45] also confirmed in this study (Figure 4). Similarities in the effects of aging freshly deposited Ni films and the incorporation Fe into Ni films on the physical characteristics of Ni suggests that Ni atoms present at the catalyst surface are the active centers involved in the evolution of O$_2$. To test this hypothesis, we compute the turnover frequency based on the number of Ni atoms in the catalyst films, TOF$_{min}$. We note that the TOFs reported in this work are lower limits, since the entirety of the film may not be accessible for oxygen evolution. (TOF$_{max}$, based on the number of Ni atoms at the surfaces of the films, is provided in section S7 of the SI.) Although the absolute value of the TOF depends on assumptions of the OER-active content of the catalyst films, the composition dependence of the TOF does not. In Figure 10a, TOF$_{min}$ is plotted versus the ratio of the band intensities for the NiOOH vibrations, I_{475}/I_{555}. This plot suggests that a NiOOH-type phase with a lower ratio of Raman peak heights yields higher OER activities. (Scatter in the plot at low I_{475}/I_{555} values, or high Fe content, is attributed to decreasing NiOOH band intensities and the presence of the 494 cm^{-1} band.) The data point for the aged Ni film is included in this correlation, suggesting that changes in the NiOOH bands, regardless of their source, are linked to the increased OER activity. This relationship is further corroborated by the Ni(OH)$_2$/NiOOH redox behavior. As seen in b and c of Figure 10, respectively, the TOF correlates with the reduction peak potential and the average oxidation state of Ni (from b and c of Figure 3, respectively). The TOF increases linearly with the potential for the reduction peak, for potentials up to 0.54 V vs Hg/HgO, and despite scatter in the data, the TOF decreases with an increase in the average oxidation state of Ni. Here again, we observe that the data point for the aged Ni film agrees with the correlations. These observations suggest that suppression of the oxidation of Ni(OH)$_2$ to NiOOH, regardless of the cause, results in higher OER activities. Stated another way, the OER activity of Ni cations is higher the lower the average oxidation state of Ni. This trend agrees with the consensus in literature that β-NiOOH, for which Ni exists as Ni^{3+}, exhibits a much higher OER activity than γ-NiOOH for which Ni exists as Ni$^{3.7+}$.[14,25−28] The results reported here suggest that further reduction in the average oxidation state of Ni by the addition of Fe results in higher OER activities which surpass that of aged Ni.

It should be noted that the Raman spectra for Ni−Fe films also show evidence of lower crystallinity and a smaller
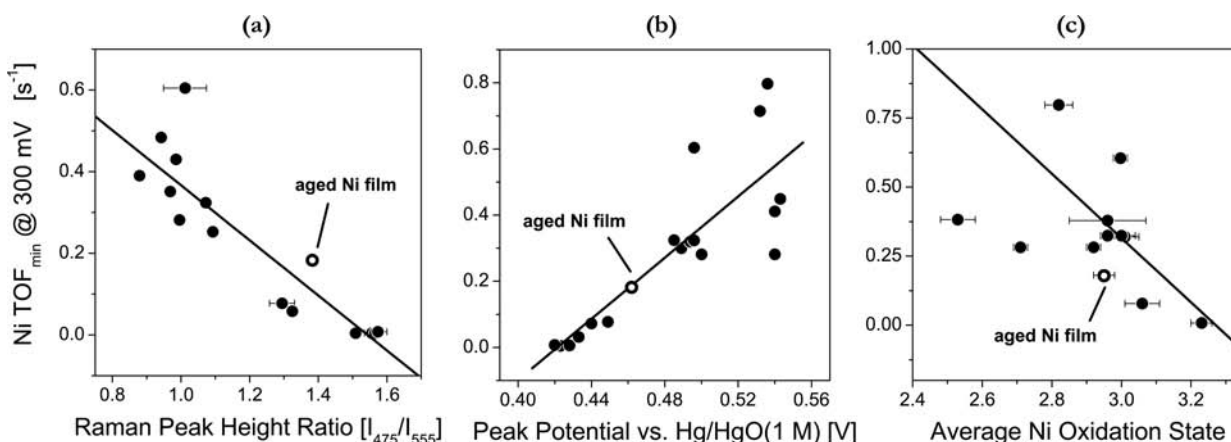
Figure 10. Turnover frequency (TOF_{min}) based on Ni sites for the OER plotted against the corresponding (a) intensity ratio of the 475 cm^{-1} band to the 555 cm^{-1} band obtained from in situ Raman spectra, (b) the NiOOH reduction peak potential, and (c) the average oxidation state of Ni. Filled markers correspond to the as-deposited Ni−Fe films, and the unfilled marker corresponds to an aged Ni film. Lines are fits to the data. The corresponding plots for the specific current densities are shown in Figure S25 of the SI.

contribution from β-Ni(OH)$_2$ with increasing Fe content at 0.2 V (Figure 7a). Furthermore, the unidentified band at 494 cm^{-1} observed at 0.6 V for Ni−Fe films with 30−80% Fe (Figure 8a) matches very well to that observed for defective Ni(OH)$_2$ (Figure 7a).[23,25,31,33−36] These observations indicate that the Ni−O vibrations which result from structural defects in Ni(OH)$_2$ are retained when Ni(OH)$_2$ is oxidized to NiOOH for films which contain a significant amount of Fe. (See additional discussion in section S5.4.1 of the SI.) The observation that these highly active Ni−Fe films are disordered is consistent with previous reports of amorphous metal oxides for the OER.[12,46] Thus, although the Ni−Fe system displays trends in NiOOH-type vibrations similar to that for the γ−β transformation, the structure of the Ni phase in Ni−Fe catalyst may not be exactly that of β-NiOOH. Previous in situ X-ray absorption spectroscopy studies[15,16] have reported the parent structure of oxidized Ni films with low Fe content (<17% Fe) to be similar to γ-NiOOH. Therefore, it is likely that Raman spectroscopy probes local characteristics of Ni−O not captured by the extended X-ray absorption fine structure (EXAFS) which, while able to provide the local structure and coordination around Ni, does not readily provide structural information beyond the Ni−O planes of layered nickel (oxy)hydroxides.[15,16,47] That is, while the Raman bands at ∼475 and ∼555 cm^{-1} are generated by the same basic structural unit, their relative intensities reflect the local structure around Ni−O which is influenced by factors including the interlayer spacing between Ni−O sheets, the presence of protons or other cations (such as potassium) between the sheets, structural disorder within sheets, and the metal oxidation state.[22] Similarly, the energetics of the Ni(OH)$_2$/NiOOH transformation may also be influenced by such factors.

The similarity in the vibrational and redox characteristics of aged Ni films and the NiOOH phase in mixed Ni−Fe films suggest that Ni−O vibration may be an indicator of the OER activity; this is consistent with the OER pathway which must involve adsorbed oxygen-based intermediates at the presumed Ni active site. The suggestion that Ni plays an active role in facilitating the OER in these catalysts is consistent with the kinetic parameters for these films. Specifically, the Tafel slope and reaction order in OH$^-$ for mixed Ni−Fe films agree with those for aged Ni films but not as-deposited Ni films or Fe films, indicating that Ni−Fe catalysts share a common reaction

pathway with aged Ni. A further implication is that, while aging of Ni films can achieve a maximum of ∼4 mA cm^{-2}, the addition of Fe to Ni can modify the Ni−O character so as to surpass the OER currents of aged Ni films by 5-fold (20 mA cm^{-2} for Ni−Fe containing ∼40% Fe). On the basis of Ni as the active site for OER, we interpret the maximum in the specific current density for the OER (Figure 2) to be a competition between the increasing activity of the Ni sites, as influenced by its Fe neighbors, and the decreasing quantity of Ni sites as more Fe is incorporated.

4. CONCLUSION

We have examined the electrochemical and structural characteristics of Ni−Fe OER catalysts across the full composition range. Electrodeposited Ni−Fe films containing 40% Fe exhibit OER current densities which are 2 orders of magnitude higher than freshly deposited Ni films and 3 orders of magnitude higher than Fe films. Electrochemical measurements show that the Ni(OH)$_2$/NiOOH redox couple shifts monotonically to higher (anodic) potentials with increasing Fe content, indicating that Fe suppresses the electrochemical oxidation of Ni(OH)$_2$ to NiOOH. Correspondingly, the number of electrons transferred during redox indicates that the average oxidation state of the nominally Ni(III) sites decreases with Fe incorporation. Characterization of the Ni−Fe films by in situ Raman spectroscopy reveals that the catalysts, particularly those exhibiting high OER activities, display some degree of disorder. Raman spectra also reveal that, under OER potentials, Ni in the Ni−Fe mixtures contain a structural unit similar to NiOOH. Furthermore, the local environment of Ni−O, as described by the relative intensities of the two NiOOH bands at 475 and 555 cm^{-1}, is modified dramatically by the presence of Fe. Both properties of the Ni−Fe films, that is, the redox behavior and the Raman characteristics of the NiOOH-type phase, correlate with the OER activity. This correlation is consistent with the effect of aging on Ni films; that is, aging of Ni films improves the OER activity while modifying the redox and Raman characteristics of Ni in a manner similar to that observed for Fe incorporation. Similarities between aged Ni and Ni−Fe mixtures are also supported by the observation that the Tafel slope and the reaction order in OH$^-$ for aged Ni films match those for the mixed Ni−Fe films, suggesting a common reaction

pathway. Taken together, our observations demonstrate that the local environment of Ni in Ni–Fe films strongly affects the average oxidation state and OER activity of Ni in alkaline electrolytes.

■ ASSOCIATED CONTENT

S Supporting Information

Additional experimental procedures, supplementary electrochemical data, Raman spectroscopy, X-ray photoelectron spectra. This material is available free of charge via the Internet at http://pubs.acs.org.

■ AUTHOR INFORMATION

Corresponding Author
bell@cchem.berkeley.edu

Notes
The authors declare no competing financial interest.

■ ACKNOWLEDGMENTS

■ REFERENCES

(1) Walter, M. G.; Warren, E. L.; McKone, J. R.; Boettcher, S. W.; Mi, Q. X.; Santori, E. A.; Lewis, N. S. *Chem. Rev.* **2010**, *110*, 6446.
(2) Cook, T. R.; Dogutan, D. K.; Reece, S. Y.; Surendranath, Y.; Teets, T. S.; Nocera, D. G. *Chem. Rev.* **2010**, *110*, 6474.
(3) Matsumoto, Y.; Sato, E. *Mater. Chem. Phys.* **1986**, *14*, 397.
(4) Corrigan, D. A. *J. Electrochem. Soc.* **1987**, *134*, 377.
(5) Hu, C. C.; Wu, Y. R. *Mater. Chem. Phys.* **2003**, *82*, 588.
(6) Landon, J.; Demeter, E.; Inoglu, N.; Keturakis, C.; Wachs, I. E.; Vasic, R.; Frenkel, A. I.; Kitchin, J. R. *ACS Catal.* **2012**, *2*, 1793.
(7) Li, X. H.; Walsh, F. C.; Pletcher, D. *Phys. Chem. Chem. Phys.* **2011**, *13*, 1162.
(8) Miller, E. L.; Rocheleau, R. E. *J. Electrochem. Soc.* **1997**, *144*, 3072.
(9) Potvin, E.; Brossard, L. *Mater. Chem. Phys.* **1992**, *31*, 311.
(10) Singh, R. N.; Pandey, J. P.; Anitha, K. L. *Int. J. Hydrogen Energy* **1993**, *18*, 467.
(11) Trotochaud, L.; Ranney, J. K.; Williams, K. N.; Boettcher, S. W. *J. Am. Chem. Soc.* **2012**, *134*, 17253.
(12) Smith, R. D. L.; Prevot, M. S.; Fagan, R. D.; Zhang, Z. P.; Sedach, P. A.; Siu, M. K. J.; Trudel, S.; Berlinguette, C. P. *Science* **2013**, *340*, 60.
(13) Lyons, M. E. G.; Brandon, M. P. *Int. J. Electrochem. Soc.* **2008**, *3*, 1463.
(14) Lyons, M. E. G.; Brandon, M. P. *Int. J. Electrochem. Soc.* **2008**, *3*, 1386.
(15) Kim, S. H.; Tryk, D. A.; Antonio, M. R.; Carr, R.; Scherson, D. *J. Phys. Chem.* **1994**, *98*, 10269.
(16) Balasubramanian, M.; Melendres, C. A.; Mini, S. *J. Phys. Chem. B* **2000**, *104*, 4300.
(17) Corrigan, D. A.; Conell, R. S.; Fierro, C. A.; Scherson, D. A. *J. Phys. Chem.* **1987**, *91*, 5009.
(18) Guerlou-Demourgues, L.; Fournes, L.; Delmas, C. *J. Electrochem. Soc.* **1996**, *143*, 3083.
(19) Gao, P.; Gosztola, D.; Leung, L. W. H.; Weaver, M. J. *J. Electroanal. Chem.* **1987**, *233*, 211.
(20) Yeo, B. S.; Klaus, S. L.; Ross, P. N.; Mathies, R. A.; Bell, A. T. *ChemPhysChem* **2010**, *11*, 1854.
(21) Trasatti, S.; Petrii, O. A. *Pure Appl. Chem.* **1991**, *63*, 711.
(22) Kostecki, R.; McLarnon, F. *J. Electrochem. Soc.* **1997**, *144*, 485.
(23) Yeo, B. S.; Bell, A. T. *J. Phys. Chem. C* **2012**, *116*, 8394.
(24) Doyle, R. L.; Lyons, M. E. G. *J. Electrochem. Soc.* **2013**, *160*, H142.
(25) Oliva, P.; Leonardi, J.; Laurent, J. F.; Delmas, C.; Braconnier, J. J.; Figlarz, M.; Fievet, F.; Deguibert, A. *J. Power Sources* **1982**, *8*, 229.
(26) Desilvestro, J.; Corrigan, D. A.; Weaver, M. J. *J. Electrochem. Soc.* **1988**, *135*, 885.
(27) Fu, X. Z.; Zhu, Y. J.; Xu, Q. C.; Li, J.; Pan, J. H.; Xu, J. Q.; Lin, J. D.; Liao, D. W. *Solid State Ionics* **2007**, *178*, 987.
(28) Cordoba-Torresi, S. I.; Gabrielli, C.; Hugotlegoff, A.; Torresi, R. *J. Electrochem. Soc.* **1991**, *138*, 1548.
(29) Wehrens-Dijksma, M.; Notten, P. H. L. *Electrochim. Acta* **2006**, *51*, 3609.
(30) Godwin, I. J.; Lyons, M. E. G. *Electrochem. Commun.* **2013**, *32*, 39.
(31) Johnston, C.; Graves, P. R. *Appl. Spectrosc.* **1990**, *44*, 105.
(32) Bernard, M. C.; Cortes, R.; Keddam, M.; Takenouti, H.; Bernard, P.; Senyarich, S. *J. Power Sources* **1996**, *63*, 247.
(33) Cornilsen, B. C.; Shan, X. Y.; Loyselle, P. L. *J. Power Sources* **1990**, *29*, 453.
(34) de Torresi, S. I. C.; Provazi, K.; Malta, M.; Torresi, R. M. *J. Electrochem. Soc.* **2001**, *148*, A1179.
(35) Vidotti, M.; Salvador, R. P.; de Torresi, S. I. C. *Ultrason. Sonochem.* **2009**, *16*, 35.
(36) Vidotti, M.; Salvador, R. P.; Ponzio, E. A.; Cordoba de Torresi, S. I. *J. Nanosci. Nanotechnol.* **2007**, *7*, 3221.
(37) Kostecki, R.; McLarnon, F. In *Proceedings of the Symposium on Electrode Materials and Processes for Energy Conversion and Storage IV*; McBreen, J., Mukerjee, S., Srinivasan, S., Eds.; Electrochemical Society, Inc.: Pennington, NJ, 1997; p viii.
(38) Bernard, M. C.; Bernard, P.; Keddam, M.; Senyarich, S.; Takenouti, H. *Electrochim. Acta* **1996**, *41*, 91.
(39) Hibben, J. H. *J. Chem. Phys.* **1937**, *5*, 166.
(40) Cornell, R. M.; Schwertmann, U. *The Iron Oxides: Structure, Properties, Reactions, Occurrences, and Uses*, 2nd completely rev. and extended ed.; Wiley-VCH: Weinheim, 2003.
(41) Thierry, D.; Persson, D.; Leygraf, C.; Boucherit, N.; Hugotlegoff, A. *Corros. Sci.* **1991**, *32*, 273.
(42) Graves, P. R.; Johnston, C.; Campaniello, J. J. *Mater. Res. Bull.* **1988**, *23*, 1651.
(43) Jacob, J.; Khadar, M. A. *J. Appl. Phys.* **2010**, *107*, 114310.
(44) Lu, P. W. T.; Srinivasan, S. *J. Electrochem. Soc.* **1978**, *125*, 1416.
(45) Cappadonia, M.; Divisek, J.; Vonderheyden, T.; Stimming, U. *Electrochim. Acta* **1994**, *39*, 1559.
(46) Merrill, M. D.; Dougherty, R. C. *J. Phys. Chem. C* **2008**, *112*, 3655.
(47) Pandya, K. I.; Hoffman, R. W.; McBreen, J.; O'Grady, W. E. *J. Electrochem. Soc.* **1990**, *137*, 383.